Mini Review

JOURNAL OF THE CHINESE CHEMICAL SOCIETY

Transient Infrared Absorption Spectra of Reaction Intermediates Detected with a Step-scan Fourier-transform Infrared Spectrometer

Yu-Hsuan Huang,[a] Jin-Dah Chen,[a] Kuo-Hsiang Hsu,[a] Li-Kang Chu[b]* and Yuan-Pern Lee[a,c]*

[a]*Department of Applied Chemistry and Institute of Molecular Science, National Chiao Tung University, 1001, Ta-Hsueh Road, Hsinchu 30010, Taiwan*

[b]*Department of Chemistry, National Tsing Hua University, 101, Sec. 2, Kuang-Fu Rd., Hsinchu 30013, Taiwan*

[c]*Institute of Atomic and Molecular Sciences, Academia Sinica, Taipei 10617, Taiwan*

(Received: Aug. 9, 2013; Accepted: Sept. 23, 2013; Published Online: Oct. 22, 2013; DOI: 10.1002/jccs.201300415)

Our group has utilized a step-scan FTIR spectrometer operating in the absorption mode to characterize transient species in chemical reactions upon photo-irradiation of gaseous mixtures in a multipass White cell. The operational temporal resolution is typically 1–10 μs with spectral resolution 0.1– 4 cm^{-1}, depending on conditions. The acquisition of both ac- and dc-coupled signals enables an extraction of minute changes in the large background signal to attain a typical detectable absorbance variation greater than 1×10^{-4}. By consideration of reaction mechanisms and comparison of vibrational wavenumbers, IR intensities, and rotational contours predicted with theoretical calculations, we have assigned IR absorption bands of many important atmospheric free radicals and unstable species including their conformers, such as ClCO, ClSO, ClCS, ClCOOH, CH_3SO_2, CH_3SOO, CH_3OSO, CH_3SO, CH_3OO, $CH_3C(O)OO$, CH_2OO C_6H_5CO, $C_6H_5SO_2$, and $C_6H_5C(O)OO$. The advantages and limitations of this technique to perform spectral and kinetic investigations of transient species in chemical reactions are discussed.

Keywords: Step-scan; Fourier-transform infrared spectroscopy; Transient absorption; FTIR; Free radicals.

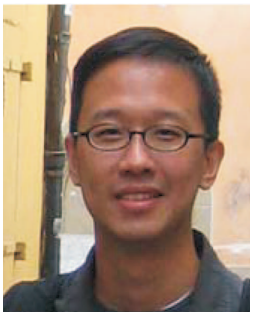

Li-Kang Chu*: B. S. (2000) and Ph.D. (2006) in chemistry, National Tsing Hua University, Taiwan. Postdoctoral researcher, Laser Dynamics Lab, Georgia Institute of Technology (2008-2010). Assistant professor, Department of Chemistry, National Tsing Hua University, Taiwan (2010-). His main research interests focus on the spectroscopy, kinetics, and ion pumps of the photosynthetic proteins, using various time-resolved approaches including step-scan FTIR, nanosecond-resolved transient absorption, and electrochemical methods.*

Yuan-Pern Lee*: B. S. in chemistry, National Taiwan University (1973) and Ph.D. in chemistry, University of California, Berkeley (1979). Postdoctoral fellow, Aeronomy Laboratory, NOAA, Boulder, Colorado. Associate professor (1981-1985) and professor (1985-2004), Chemistry Department, National Tsing Hua University, Taiwan. Adjunct research fellow, Institute of Atomic and Molecular Sciences, Academia Sinica (1987-). Chair professor, Department of Applied Chemistry (2004-), Dean of Science (2005-2008), and Director of Center for Interdisciplinary Science (2006-), National Chiao Tung University. The main research topics pursued concern spectroscopy, kinetics and dynamics of free radicals or unstable species, using diverse methods including step-scan time-resolved FTIR (emission or absorption), matrix isolation using p-H_2, cavity ringdown, IR-VUV photoionization, and ultrafast lasers. He has identified more than 70 new free radicals, most of which are important in atmospheric, combustion, or planetary chemistry. He has received numerous honors, and was elected as Fellow of the American Physical Society in 1999, National Chair Professor from Ministry of Education (since 1997), Academician of Academia Sinica in 2008, and fellow of TWAS-academy of sciences for the developing world in 2011.*

Special Issue for the 60th Anniversary of Journal of the Chinese Chemical Society

* Corresponding author. Tel: +886-3-5131459; Fax: +886-35713491; Email: lkchu@mx.nthu.edu.tw (L.-K. Chu) and yplee@mail.nctu.edu.tw (Y.-P. Lee)

INTRODUCTION

Infrared absorption spectra, which are regarded as molecular fingerprints, have been employed extensively in environmental sciences, atmospheric chemistry, analytical chemistry, and industrial applications. The conventional continuously scanned (cs) Fourier-transform infrared (FTIR) spectrometer utilizes a continuous-scan Michelson interferometer to record the interferogram (a plot of intensity as a function of optical path difference); an interferogram yields a conventional spectrum (a plot of intensity as a function of wavelength λ or wavenumber σ) via Fourier transformation. The FTIR technique possesses several advantages such as multiplex,[1] large throughput,[2] great accuracy of wavenumber,[3] and superb spectral resolution; the FTIR spectrometer has hence become a standard instrument in modern chemical laboratories. Because the interferogram of the cs-FTIR spectrometer is recorded on scanning the mirror in one arm of the divided beam in the interferometer to create an optical path difference, the best temporal resolution achievable is ~5 ms when a rapid-scan mode is employed.[4] Such a temporal resolution is unsatisfactory for the detection of transient species that might have a typical lifetime less than 0.2 ms. Several methods have been developed to overcome this limitation to record IR spectra with improved temporal resolution.[5] Among them, an interferometer operated in the step-scan (or stop-scan, ss) mode,[6] in which the moving mirror scans in a discrete fashion, is the most promising approaches to achieve this objective.[7,8]

Initially, the ss-FTIR instrument was employed in an emission mode to investigate the chemical dynamics of photodissociation and chemical reactions.[9–17] Green *et al.* investigated the vibrational relaxation of excited NO by O_2.[9] Hancock and Heard investigated the chemiluminescence from the reaction of O (^{3}P) + CF_2 ($\tilde{X}\ ^1A_1$) with spectral resolution 2 cm^{-1} and temporal resolution 10 ns.[10] Hartland *et al.* investigated the laser induced fluorescence of I_2 and achieved spectral resolution of 0.25 cm^{-1} and temporal resolution of 100 ns.[11] In our laboratory we employed the ss-FTIR emission spectroscopy to study the photodissociation dynamics of various haloethenes, such as vinyl halides,[12,13] CH_2CF_2,[14] and CF_2CHCl (Ref. 15) as well as chemical reactions of Cl + CH_3SH (Ref. 16) and Cl + H_2S (Ref. 17) on monitoring the emission of HF or HCl to derive their vibration-rotational energy distributions. Our detection scheme subsequently extended to emission of CO,[18–23] CO_2 (Ref. 24, 25), HCO,[23] OH,[22,26] and NO.

The ss-FTIR technique in absorption mode has been used in the condensed phase for the investigation of photochemistry of photosynthetic proteins,[27,28] metallic complexes,[29,30] and species in zeolites[31] and in bio-systems.[32] In contrast, to our knowledge, reports on investigations of gaseous reactive species using ss-FTIR technique in absorption mode are only from our laboratory. Since our first launch of this technique to detect the IR absorption spectrum of gaseous ClCO in 2001,[33] we have continuously improved the technique to observe many important radicals and reactive species, including ClSO,[34] ClCS,[35] CH_3SO_2,[36] $C_6H_5SO_2$,[37] ClCOOH,[38] CH_3SOO,[39] CH_3SO,[39] CH_3OSO,[40] CH_3OO,[41] $CH_3C(O)OO$,[42] C_6H_5CO,[43] $C_6H_5C(O)OO$,[44] and, most excitingly, the simplest Criegee intermediate, CH_2OO.[45]

In this review, we describe the basic principles and instrumentation of using an ss-FTIR spectrometer to record transient absorption spectra, the methods to identify transient species with spectral assignments, and some representative results; the advantages and limitations of this technique are also discussed.

EXPERIMENTS

Data acquisition using an ss-FTIR spectrometer

Unlike a conventional FTIR spectrometer, in which a mirror moves continuously during the scan to produce an interferogram, an ss-FTIR spectrometer records a signal as the moving mirror stops at specific points defined by the zero crossing of the He-Ne laser fringes. Figure 1 depicts the data acquisition of an ss-FTIR spectrometer. The abscissa represents the position at which the moving mirror stops, and the other two axes represent the time evolution (t) and intensity (I) of the detected signal. After the moving mirror is stopped and stabilized at a given position x_i, corresponding to an optical path difference s_i, the temporal profile, denoted as $I_{si}(t_n)$, is recorded at specified intervals after being initiated by a triggered event, typically a laser irradiation. Gener-

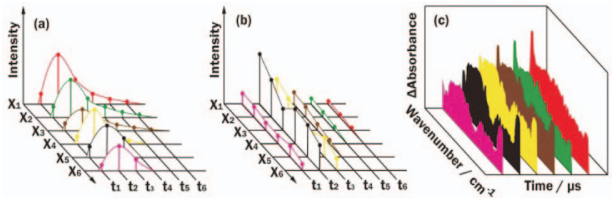

Fig. 1. Schematic diagram of the data acquisition of a step-scan FTIR spectrometer. (a) Temporal profiles at varied steps x_i are recorded. (b) Interferograms at varied intervals t_i after the rearrangment of (a). (c) Time-resolved spectra are obtained upon Fourier transformation.

ally 10-100 temporal profiles are recorded for signal averaging before the moving mirror becomes stepped to the next point x_{i+1}, corresponding to a path difference s_{i+1}, to repeat the acquisition of the temporal profile. After recording all temporal profiles at all steps, as shown in Fig. 1(a), matrix $I_{si}(t_n)$ is rearranged to yield the temporally-resolved interferograms, denoted as $I_{tn}(s_i)$ and shown in Fig. 1(b), corresponding to each specific period t_n after triggering. The time-resolved spectra in a set $I_{tn}(\sigma)$, shown in Fig. 1(c), are thus obtained by Fourier transformation of $I_{tn}(s_i)$.

Ac/dc detection

The interferogram of a cs-FTIR spectrometer is recorded in an ac-mode as the detector experiences modulation in signal when the mirror moves continuously to create optical path differences. In a step-scan mode, the interferogram is typically recorded in a dc-mode because the signal that the detector monitors does not vary with time as the mirror stops at a specific position; phase information is retrieved from this dc-coupled interferogram. However, to observe a minute change in a large background signal upon laser irradiation, ac-coupled detection is needed. The time-resolved absorption measurements are hence accomplished on recording both the dc- and ac-coupled signals either simultaneously or consecutively.[46,47] For consecutive measurements, the dc-coupled signal is measured first without laser excitation, followed by the time-resolved measurements of the ac-coupled signals upon laser excitation. The dc-coupled signal is used to obtain a static interferogram, $I_0(s)$, in which s is the path difference or optical retardation. Upon Fourier transformation, it then serves as the background spectrum, $S_0(s)$, and provides the phase information, $\varphi(\sigma)$. An ac-coupled signal records the changes induced by laser irradiation. After Fourier transformation of these recorded interferograms at specific time delays t_n, $I_{tn}(s_i)$, using the stored phase from the dc-coupled measurement, temporally resolved differential spectra at varied periods t, $\Delta S_t(\sigma)$ are obtained. The difference absorbance spectrum at time t, $\Delta A_t(\sigma)$, is thus expressed as

$$\Delta A_t(\sigma) = -\log\left[\frac{S_0(\sigma) + \Delta S_t(\sigma)}{S_0(\sigma)}\right] = -\log\left[1 + \frac{\Delta S_t(\sigma)}{S_0(\sigma)}\right] \quad (1)$$

In the difference spectrum, lines pointing upwards typically indicate production of new species, whereas those pointing downward indicate destruction of the precursor. Caution should be exercised to ensure that both $S_0(\sigma)$ and $S_t(\sigma)$ are adjusted to the same amplification factor if the dc- and ac-coupled signals are pre-amplified with different factors.

Undersampling

There is commonly no benefit to record an extensive spectrum when only a section of the spectral region is of interest. To decrease the duration of data acquisition, undersampling, which decreases the number of acquired interferogram points, is applied in our measurements. In the step-scan mode, the interferogram is sampled discretely, and the zero-crossing points of the interference fringes of a monochromatic HeNe laser (632.8 nm) serve as a reference for sampling. According to the Nyquist criterion,[48] any waveform that is a sinusoidal function can be sampled unambiguously with a sampling frequency greater than, or equal to, twice the bandwidth of the system. If the sampling interval is 632.8 nm, which is equivalent to 15802 cm^{-1}, the maximum (Nyquist) wavenumber range is hence 0–7899 cm^{-1}. When the spectrum is limited to a smaller spectral range, a lower sampling frequency corresponding to a larger sampling interval might be used, resulting in a smaller number of points in the interferogram. For example, for a spectrum of interest in spectral range 1053-2106 cm^{-1}, a sampling interval 15 × 632.8 nm is sufficient to record the waveform. Each data acquisition is hence performed after the moving mirror has advanced 15 steps; the number of acquisition points can thus be decreased to 1/15 of that in normal sampling. The advantage of undersampling is more pronounced for a high-resolution spectrum in a short spectral range.

Instruments

A commercial ss-FTIR spectrometer coupled with a multi-reflection White cell is employed for our time-resolved absorption measurements. Figure 2 shows the experimental setup. We discuss below the details of two major systems in our laboratory.

1a. First-generation system

The step-scan measurements are performed under the master mode of the spectrometer (Thermo Nicolet, NEXUS 870), in which the timing trigger is initiated by the spectrometer. Figure 3

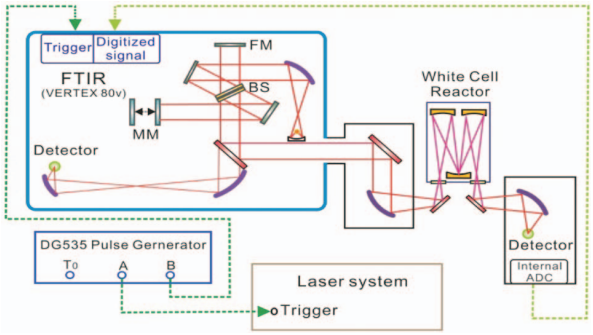

Fig. 2. Schematic diagram of experimental setup. A commercial FT-IR spectrometer coupled with a White cell reactor is used. The solid lines represent the optical path of the IR probing light and the detection at the right exit port is used for step-scan measurements. The dotted lines represent the electronic signal cabling. FM: fixed mirror; BS: beam splitter; MM: moving mirror.

shows the timing diagram of data acquisition. When the moving mirror steps to the desired position, 300-600 ms suffices to stabilize the mirror, depending on the mirror velocity and undersampling ratio. After the preset settling time *T*, the dc-coupled signal is recorded by the internal analogue-to-digital-converter (ADC, 2×10^5 sample s^{-1}, 16 bit) without amplification. The spectrometer then sends the 'take-data' signal (TKDA) to trigger an external delay generator (DG535, Stanford Research Systems). This delay generator serves to trigger the photolysis laser and the external ADC (GAGE Applied Technologies, CompuScope 14100, 10^8 sample s^{-1}, 14 bit,) to record the ac-coupled signal. The external ADC is triggered when the photolysis laser beam arrives at the flow reactor. After laser excitation, the pre-amplified ac-coupled signal is sent to a voltage amplifier (Stanford Research Systems, SR560) for further amplification (typically, gain ~10) before being recorded with the external ADC. The minimal temporal resolution, indicated as C in Fig. 3, is 10 ns for the external ADC used. In principle, the temporal resolution is limited only by the response time of the detector and the ADC; the practical temporal resolution is typically determined by the acceptable ratio of signal to noise (S/N). In our experiments we typically employed 150 slices at interval 1 μs. The TKDA signal repeats several times (typically 10–30 times in our experiments, but only 3 times are shown in Fig. 3) for averaging. After the desired acquisition at a given mirror position, the mirror moves to the next step. The maximal optical retardation, hence the maximal distance that the moving mirror travels, is determined by the spectral resolution. The highest available instrumental resolution (before apodization) of this interferometer is 0.2 cm^{-1}. In consideration of duration of measurement and stability of the system, the spectral resolution is typically set at 1-4 cm^{-1}.

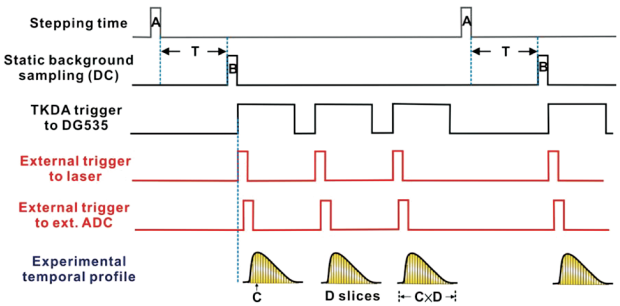

Fig. 3. Time chart of the Nexus 870 spectrometer operating in its master mode. A: stepping time of the moving mirror; T: stabilization time of the moving mirror; B: data acquisition time of the dc-coupled signal; C: temporal resolution of the analogue-to-digital converter (ADC); D: number of time slices; C×D: total period of temporal profile.

1b. Second-generation system

In our second-generation system the step-scan FTIR spectrometer (Bruker, Vertex 80v) employs all-digital electronics to improve the performance. The spectrometer is operated under an external triggering mode, whereby the timing trigger is initiated with an external delay generator (DG535). In this system, the dc-coupled background spectrum is measured first separately. The ac-coupled signal, synchronized with laser excitation, is recorded in a separate measurement. Figure 4 shows the timing diagram with external triggering. After the settling time *T* (400-600 ms), the measurement trigger is activated. The sequence trigger is activated to initiate the data acquisition only when the measurement trigger is activated and an external trigger to spectrometer initiates the process, such as E_1 in Fig. 4; otherwise, the external trigger to spectrometer is ignored, such as E_2 in Fig. 4. For this system, the ultimate temporal resolution is 5 ns for an external ADC (MI3025, 2×10^8 sample s^{-1}, 12 bit), but an internal ADC (8×10^4 sample s^{-1}, 24 bit) at 12.5-μs resolution is typically used for its greater dynamic range; a resolution 6.3 μs for the latter is also available. Both the preamplified dc- and ac-coupled signals are recorded by the internal ADC without further amplification. The greatest instrumental resolution of this instrument (without apodization) is 0.083 cm^{-1}. With this resolution and much improved S/N of the system, we have demonstrated that rotational lines in an IR band become partially resolved, to be discussed below.

2. Multipassing absorption cell and reactor

A White cell[49] is mounted vertically in the sample compartment of the spectrometer to serve as the flow reactor. The body is made of stainless steel with an interior volume of ~1.5 L and is

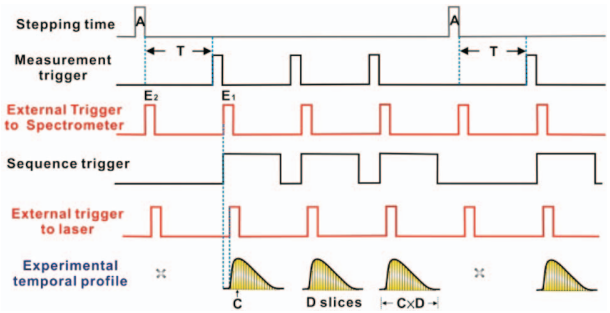

Fig. 4. Time chart of the Vertex80v spectrometer operating in its external-trigger mode. A: stepping time of the moving mirror; T: stabilization time of the moving mirror; E_1: external trigger to the spectrometer activated by the measurement trigger; E_2: external trigger to the spectrometer that is ignored; C: temporal resolution of the analogue-to-digital converter (ADC); D: number of time slices.

equipped with a water jacket to perform experiments at varied temperature. The White cell contains two concave spherical mirrors with the same radius of curvature, which defines the distance between them; one mirror is cut into halves for adjustment of the tilt between them. Figure 5 shows the structure of the White cell. The probing IR light reflects several times to increase the optical path, hence the absorbance. White cells with a base path of length 20 cm with a maximal effective absorption length 6.0 m, and a base path length 15 cm with a maximal effective absorption length 3.6 m are used in our measurements. Parallel to the IR paths, two rectangular quartz windows (3×12 cm^2) on two sides of the chamber are mounted to allow passage of the photolysis laser beam, which propagates through these windows and is multiply reflected between a pair of rectangular laser mirrors installed externally but nearly parallel to the quartz windows. The photolysis wavelengths vary with the chemical systems of interest; we generally use light at 193 and 248 nm from an excimer laser and at 355 nm from the third-harmonic output of a Nd:YAG laser.

3. Key factors in experiments

In experiments for detection of unstable intermediates, two factors should be considered: S/N and temporal resolution. Many factors affect the S/N: stability of the mirrors, acoustic noise, flow turbulence in the reactor, electric connections of the detector signal, and electromagnetic noise from the photolysis laser. Care must be taken to minimize all these factors to achieve a satisfactory S/N.

If one can control the reaction kinetics so that the intermediate endures more than 100 μs, integration of the spectra over an extended period helps to improve the S/N. When employing a non-integrating ADC, one should perform data acquisition at the greatest rate and integrate the data to the desired temporal resolution to improve the S/N.

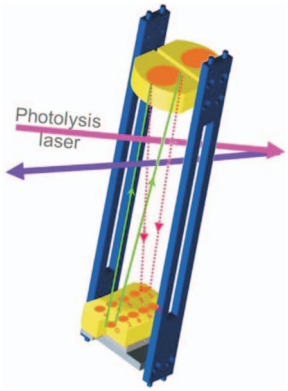

Fig. 5. Schematic of the White cell. The first and second IR beam paths and the first and second UV photolysis beam paths of the multiply reflected light are shown. Circular dots indicate images of the IR beam at each reflection.

In step-scan measurements, the stability of the moving mirror is also critical to the S/N of the spectrum. If the moving mirror is not held in position stably, slight dithering might cause an artificial signal, especially for the ac-coupled signal. Before each experiment, one has to measure the actual settling time of the mirror and set the settling time properly, especially when a large factor of undersampling is employed. As one records a high-resolution spectrum, extensive undersampling is necessary to keep the duration of data acquisition within a reasonable period. Two important aspects must be addressed when undersampling is used. First, an appropriate optical filter must be employed to confine light to the desired spectral range to reach the detector; otherwise, folding or aliasing from other spectral range might appear in the resultant spectrum to interfere with the original spectrum.[50] Second, because the mirror travels a greater distance before it stops, a greater settling time should be used for the moving mirror when extensive undersampling is applied.

RESULTS AND DISCUSSION

Methods to produce reaction intermediates

The unstable gaseous reaction intermediates are typically produced by either direct photodissociation of a precursor or via a bimolecular reaction of photolyzed reactants. In both cases, the excess energy of the products after irradiation or reaction should be rapidly removed; otherwise, the highly unstable intermediates might further dissociate. Some precursors that might not dissociate upon irradiation are in their internally highly excited states; the side lobes of the parent absorption bands due to absorption of these internally excited states thus created might interfere with the detection of the intermediates. For these reasons, a buffer gas at pressure 50-200 Torr is typically added to quench the internally excited states of the products and the parent. N_2 and CO_2 are commonly used for their quenching efficiencies greater than those of inert gases. In some measurements, a buffer gas at a large pressure serves as both reactant and quencher; for example, O_2 in the peroxide measurements.

When a molecular complex produced from a termolecular reaction is desired, performing the reaction at low temperature helps to stabilize the intermediates. In contrast, higher temperature might be needed when the vapor pressure of the precursor is small under ambient conditions.

Identification of reaction intermediates

To identify the newly formed species, we typically

consider the following factors: reaction kinetics, observed vibrational wavenumbers, relative IR intensities, and rotational contours; all items are critical in the assignments of absorption bands.

With the advantage of time-resolved spectra, a temporal trace of the reactants and products can assist the identification. The temporal evolution of each spectral band can be extracted from the 3D spectra to derive the rate coefficient according to a proposed kinetic model. On comparing the temporal profiles, one can evaluate whether the mechanism of formation of the species of interest agrees with the kinetic model. Varied experimental conditions might result in varied temporal profiles of species of interest to assist the assignment. For one to confirm the identity of a newly formed species, producing it via varied precursors and via varied reaction schemes is desirable. For example, the photolysis of $(CH_3)_2CO/O_2$ at 248 nm and $CH_3CHO/O_2/Cl_2$ at 355 nm both give rise to the the same transient features, attributed to $CH_3C(O)OO$,[42] because CH_3CO is the common intermediate in both reactions and it reacts with excessive O_2 readily.

The equilibrium geometry, vibrational wavenumbers, IR intensities and rotational parameters of an unstable species in its ground and vibrationally excited ($v_i = 1$) states were calculated with the density-functional theory using GAUSSIAN 09;[51] the B3LYP method with an aug-cc-pVTZ basis set is typically employed. Analytic first derivatives are utilized in geometry optimization, and vibrational wavenumbers are calculated analytically at each stationary point. The predictions of the corresponding anharmonic wavenumbers are also carried out by calculating the analytical second derivatives. To identify the carrier of the spectrum, one typically compares the observed vibrational wavenumbers and relative IR intensities with the anharmonic vibrational wavenumbers and IR intensities predicted for all possible candidates in the reaction scheme. When the spectral patterns are similar for two possible candidates, especially two conformers, we require information on rotational contours to differentiate them.

Using the predicted molecular parameters for the ground and the vibrationally excited state, vibration-rotational spectra are simulated with the help of programs for that purpose, such as PGOPHER[52] and SpecView.[53] The rotational contours of possible candidates are compared for a final identification. As an example, *cis*-$CH_3C(O)OO$ and *trans*-$CH_3C(O)OO$ have similar vibrational wavenumbers for the C=O stretching mode, predicted near 1862 and 1851 cm^{-1}, respectively, but the *cis*-isomer has a *b*-type band for this mode whereas the *trans*-isomer has a mixed *a*-/*b*-type band. From the observed contour, we readily assign that the major carrier of this band is *trans*-$CH_3C(O)OO$; a small discrepancy can be taken into account with a small contribution from *cis*-$CH_3C(O)OO$, as shown in Fig. 6.[42]

With the second-generation system, we can partially resolve the rotational lines to make the assignments even more definitive. Some examples (spectra of ClCO and CH_3OO) illustrating this improvement will be discussed in latter sections. The best resolution achievable, 0.083 cm^{-1}, provides a chance to derive approximate primary rotational parameters *A*, *B* and *C*, especially when the parameters of the ground state are known.

Advantages and limitations

Although the ss-FTIR possesses advantages with multiplex and high throughput, its sensitivity is still unsatisfactory. To detect reactive intermediates, one can typically detect an absorbance difference greater than 10^{-4}; for most species that value corresponds to ~10^{13} molecule cm^{-3} in the reactor, still much greater than the detection limits of

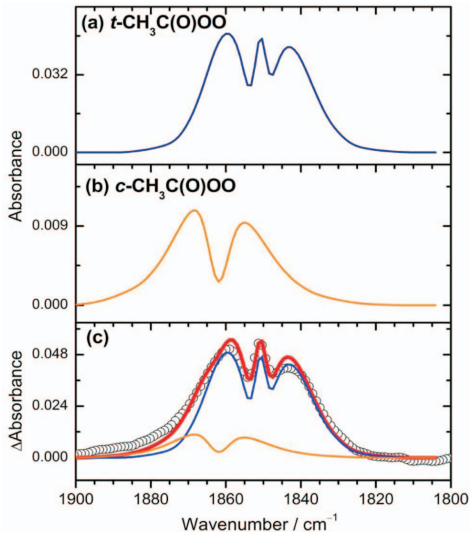

Fig. 6. Comparison of observed and simulated spectra of the C=O stretching mode of $CH_3C(O)OO$ in the region 1800–1900 cm^{-1}. (a) Simulated band of *t*-$CH_3C(O)OO$ (ν_0 = 1851 cm^{-1} and *a*-type/*b*-type = 54/46). (b) Simulated band of *c*-$CH_3C(O)OO$ (ν_0 = 1862 cm^{-1} and *a*-type/*b*-type = 1/99). (c) Comparison of spectra (open circles) observed from an irradiated flowing mixture of $CH_3CHO/Cl_2/O_2$ (2/5/500 at 100 Torr) at 298 K and simulated spectrum (thick solid line) for *t*-$CH_3C(O)OO$: *c*-$CH_3C(O)OO$ = 3.7 : 1.0; individual contributions are also shown.

other spectral techniques such as laser-induced fluorescence. For IR spectral detection, the coupling of a diode laser, an IR optical parametric oscillator/amplifier, or a quantum-cascade laser with a multipass absorption cell or a ringdown cavity provides much improved sensitivity. Nevertheless, the ss-FTIR technique possesses some advantages unsurpassed by these highly sensitive techniques mentioned above. The wide spectral coverage enables one to monitor simultaneously nearly all species in the reactor with satisfactory temporal resolution, providing ample information on the chemical kinetics that might be critical in the assignments of the spectral features and understanding the reaction mechanism. The multiplex feature of a FTIR spectrometer is also superior to the laser techniques if the laser source or the reaction system is unstable. In contrast, the laser techniques can only detect one wavelength at a time; instability of the system is more susceptible to be taken as the real signal.

The matrix-isolation technique, especially using *p*-H_2 as a host, has been commonly employed in trapping free radicals; the IR absorption spectra provide a valuable tool for the identification of these free radicals.[54,55] This technique suffers, however, from matrix shifts that causes small deviations in band positions from those in the gas-phase. With only information of vibrational wavenumbers and relative IR intensities, but without rotational contours, it might be difficult to provide definitive assignments of the observed absorption bands, especially for conformers. As discussed previously, the ss-FTIR method can utilize rotational contours as important information for band assignments. Furthermore, the lack of temporal resolution in matrix isolation prevents its study of rapidly decaying species and investigation of rapid reaction kinetics.

Another limitation of an ss-FTIR system is that the flow system uses reagents in large quantities. Unlike matrix isolation, which requires only a minute amount of sample, investigations with isotopes or valuable samples are costly and often unlikely with the ss-FTIR method. Finally, even though a resolution 0.08 cm^{-1} is attainable, this extent is still inadequate to resolve rotational fine structure. In this respect, the IR laser beams have much narrower width and enable the recording of high-resolution spectra.

Because the IR probe beam and the UV photolysis beam have disparate paths, care must be exercised to distinguish the average concentration in the IR-probed volume from the average concentration in the photolyzed volume. The concentration of IR-probed volume might be derived from the decrease in concentration of the precursor and the known or estimated yield for production of the intermediate. It can also be estimated from the theoretically predicted IR intensities; to minimize the errors due to theoretical predictions, as many bands as possible should be employed. For estimation of the concentration in a photolyzed volume, one typically has to rely on UV absorption cross sections of the precursors and the laser fluence. As diffusion is generally slower than reaction, the concentration of the photolyzed volume is used in kinetic analysis.

Significance of experimental results

We have employed the ss-FTIR technique to investigate the IR spectra and reaction kinetics of many gaseous unstable species, mostly free radicals that are important in atmospheric chemistry. Nearly all spectra recorded with this technique are previously unreported. Here we briefly describe some representative results and their significance.

1. Chlorine-containing compounds

In the degradation of chloro-hydrocarbons, several reactive Cl-containing species, such as ClCO and ClCOOH, are important intermediates in the upper atmosphere. Upon irradiation of the gaseous mixture containing Cl_2, CO, and Ar at 355 nm, the transient absorption of ClCO was observed near 1884 cm^{-1}, as shown in Figure 7 (c) with its rotational contour unresolved.[33] With the second-generation system, we have partially resolved the rotational lines of ClCO at resolution 0.083 cm^{-1}, as shown in Figure 7 (a), thus enabling a comparison of the simulated spectrum and

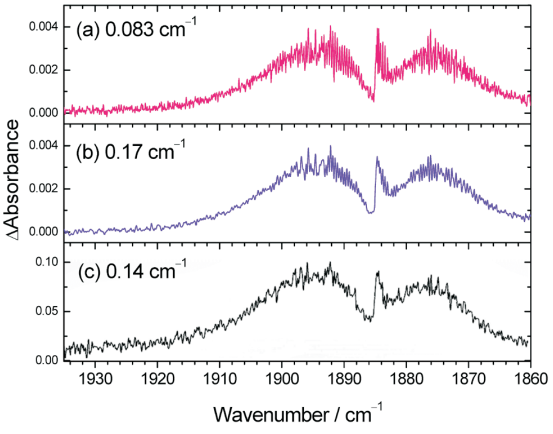

Fig. 7. Absorption spectra of ClCO recorded under varied conditions. (a) and (b) are recorded by the second-generation system at resolutions 0.083 cm^{-1} and 0.17 cm^{-1}, respectively. (c) Previous results recorded at resolution 0.14 cm^{-1} (adapted from Ref. 33; the y-axis scale might be in error).

deriving information about the structure of ClCO.

After the reaction of Cl with formic acid (HCOOH), the isomeric products *c*-ClCOOH and *t*-ClCOOH were identified;[38] ClCOOH was produced via rapid reactions of COOH with Cl_2 and Cl. Upon irradiation of the mixture of Cl_2/HCOOH/N_2, two sets of transient features were observed. Band origins at 1808.0 and 1328.5 cm^{-1} are attributed to the C=O stretching and the COH bending modes of *t*-ClCOOH, respectively, whereas those at 1883.0 and 1284.9 cm^{-1} are assigned as the corresponding modes of *c*-ClCOOH. The observed relative intensities indicate that *t*-ClCOOH is more stable than *c*-ClCOOH by ~3 kJ mol^{-1}, consistent with theoretical calculations.

We have also accomplished the detection of ClSO and ClCS upon photolysis of precursors Cl_2SO and Cl_2CS with an excimer laser.[34,35] Much buffer gas, such as Ar, N_2, CO_2, was added to the system to quench and to stabilize both the primary photolysis products and the precursor. If the quenching is insufficient, the energized primary product might undergo further dissociation and hot bands of ClSO, Cl_2SO, ClCS, and Cl_2CS appeared.

2. Important intermediates in atmospheric sulfur oxidation

The oxidation of CH_3S plays an important role in the degradation of reduced sulfur compounds, such as CH_3SCH_3, CH_3SSCH_3, and CH_3SH.[56,57] According to results of Zhu and Bozzelli, the reaction of CH_3S with O_2 yields the thermodynamically favored species CH_3SO_2 via an intermediate CH_3SOO.[58] Formation of a third isomer CH_3OSO was also predicted.[59,60] Before our work, CH_3SO_2 was detected only with a mass spectrometer; no spectral information on any isomer was available. We have prepared CH_3SO_2, CH_3OSO, and CH_3SOO from varied precursors and obtained their IR spectra.

Upon irradiation at 248 nm of a flowing mixture of CH_3SSCH_3 in excessive O_2 at 260 K, several features were observed in separate reaction periods, as shown in Fig. 8. Two transient bands with sharp Q-branches near 1397 (B) and 1110 (A) cm^{-1} were attributed to the antisymmetric CH_3-deformation and O=O stretching modes of *syn*-CH_3SOO, respectively. A band with an origin near 1071 (C) cm^{-1} appeared at a slightly later stage and was assigned to the S=O stretching mode of CH_3SO, produced via a secondary reaction of CH_3SOO with CH_3S. At an even later stage, two bands near 1170 (D) and 1120 (E) cm^{-1} were tentatively assigned to $CH_3S(O)OSCH_3$ and $CH_3S(O)S(O)CH_3$, which are probably generated via the self-reaction of CH_3SOO. The final product SO_2 was observed to increase in intensity throughout the reaction period.

Upon irradiation at 248 nm of a flowing mixture of CH_3I, SO_2 and CO_2, two transient bands near 1280 and 1076 cm^{-1} observed in the earlier stage were attributed to CH_3SO_2; a band near 1159 cm^{-1} observed in a subsequent stage was assigned to the secondary reaction product CH_3SO_2I.[37] The kinetic analysis revealed that the rate coefficient of the bimolecular reaction $CH_3 + SO_2$ is $(2.6 \pm 0.5) \times 10^{-13}$ cm^3 $molecule^{-1}$ s^{-1}, consistent with a previous report.[61] Isomer CH_3OSO was not observed in the reaction $CH_3 + SO_2$. CH_3OSO was detected upon photodissociation of $CH_3OS(O)Cl$ in CO_2 or N_2 at 248 nm.[40] Five transient features at 2991, 2956, 1154, 1151, and 994 cm^{-1} are assigned as the CH_3 antisymmetric stretching (ν_2), CH_3 symmetric stretching (ν_3), the S=O stretching mixed with CH_3 rocking (ν_8), the S=O stretching mixed with CH_3 wagging (ν_9), and the C–O stretching (ν_{10}) modes of *syn*-CH_3OSO.

Table 1 presents a summary of observed bands of CH_3SO_2, CH_3OSO, CH_3SOO, and CH_3SO. With this information, further kinetic and mechanistic investigations by direct probe of absorption bands of these S-containing radicals are possible. An example is shown in Fig. 9 in which the preliminary results clearly indicate that CH_3SO, indicated with B, and CH_3SNO_2 (A_i), CH_3SO_3H (MSA), and NO (not shown) were produced in the $CH_3S + NO_2$ reaction, initiated by photolysis at 248 nm of a mixture of $CH_3SSCH_3/NO_2/N_2$ at 16 Torr.

3. Spectra of peroxides and formaldehyde oxide

Alkyl peroxides are important intermediates in the oxidation of hydrocarbons; they are involved in catalytic cycles of ozone destruction and might be the precursors of

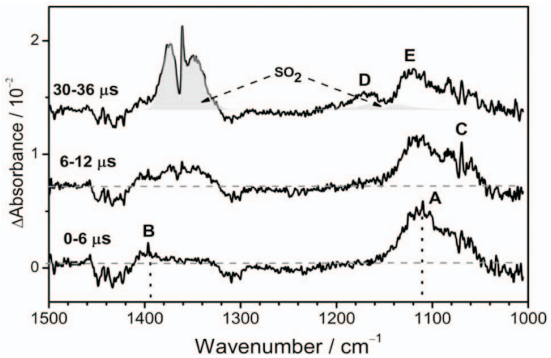

Fig. 8. Time-resolved spectra recorded at varied intervals upon irradiation of a flowing mixture of CH_3SSCH_3/O_2 at 220 Torr and 260 K (adapted from Ref. 39). A and B: CH_3SOO; C: CH_3SO; D and E: $CH_3S(O)OSCH_3$.

Table 1. Comparison of observed vibrational wavenumbers (cm^{-1}) of CH_3SO and various isomers of CH_3SO_2

CH_3SO_2		*syn*-CH_3OSO		*syn*-CH_3SOO		CH_3SO	
Cal.[a]	Expt.	Cal.[a]	Expt.	Cal.[a]	Expt.	Cal.[a]	Expt.
1262	1280	3129	2991	1459	1431	1081	1071
1074	1076	3046	2956	1425	1397		
		1166	1154	1197	1110		
		1162	1151				
		1028	994				
Ref. 36		Ref. 40		Ref. 39		Ref. 39	

[a] Harmonic vibrational wavenumbers were predicted with the B3P86 method.

smog or aerosols in the atmosphere. We produced CH_3OO upon irradiation at 248 nm of a flowing mixture of CH_3I and O_2.[41] Although some bands were overlapped, we were able to deconvolute the spectra and to identify transient absorption bands with origins near 3033, 2954, 1453, 1408, 1183, 1117, 3020, and 1441 cm^{-1}, corresponding to ν_1–ν_6, ν_9, and ν_{10} modes of CH_3OO, respectively; these values are consistent with the reported wavenumbers of CH_3OO isolated in an Ar matrix.[62] We employed the second-generation system and improved significantly the spectra both in resolution and S/N. Figure 10 shows, in the CH-stretching region, the Q-branches of ν_2 and ν_9 are clearly visible at 2954.1 and 3021.4 cm^{-1}, whereas in the previous report[41] they were derived from spectral deconvolution and comparison with simulated rotational contours.

The reaction of acetyl radical (CH_3CO) with O_2 was also investigated.[42] $CH_3C(O)OO$ is regarded as the main precursor of the peroxyacetyl nitrate (PAN), which is a major pollutant in photochemical smog.[63] We generated $CH_3C(O)OO$ on irradiation at 248 nm of a mixture of CH_3COCH_3 and O_2 or on irradiation at 355 nm of a mixture $CH_3COH/Cl_2/O_2$. The band origins near 1851, 1372, 1169, and 1102 cm^{-1} are assigned to *t*-$CH_3C(O)OO$, and those near 1862, 1142, and 1078 cm^{-1} to *c*-$CH_3C(O)OO$; a partial spectrum in the C=O stretching region is shown in Fig. 6. Our observations are consistent with those reported in an Ar matrix.[64] Use of the theoretically predicted IR intensities with the observed relative absorbance indicated that *t*-$CH_3C(O)OO$ is more stable than *c*-$CH_3C(O)OO$ by 3 ± 2 kJ mol^{-1}. A weak band near 1960 cm^{-1} assigned to *cyc*-$CH_2C(O)O$ (-lactone) is the first direct identification of the co-product of the OH-formation channel in the reaction $CH_3CO + O_2$.

Criegee intermediates are carbonyl oxides that play key roles in the reactions of ozone with unsaturated hydrocarbons; these reactions thus become an important mechanism for the removal of unsaturated hydrocarbons and for the production of OH in the troposphere. They are also responsible for the production of some acids and carbonyl compounds that might generate aerosols that contribute to local photochemical smog and global climate change. No

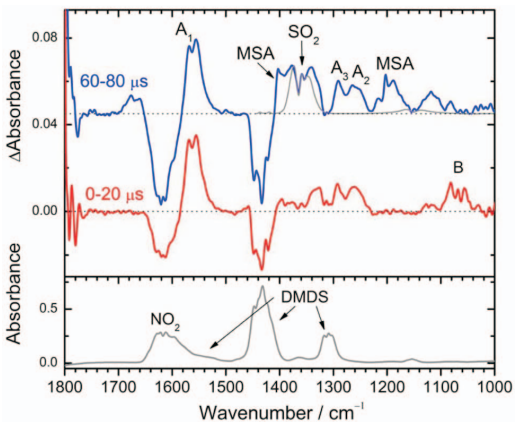

Fig. 9. Time-resolved spectra recorded at varied intervals upon irradiation at 248 nm of a flowing mixture of $CH_3SSCH_3/NO_2/N_2$ (0.9/0.09/15 at 16.2 Torr and at 298 K) in the region 1000–1800 cm^{-1}. Bottom: before photolysis (DMDS indicates CH_3SSCH_3); A_1–A_3: CH_3SNO_2; B: CH_3SO; MSA: CH_3SO_3H.

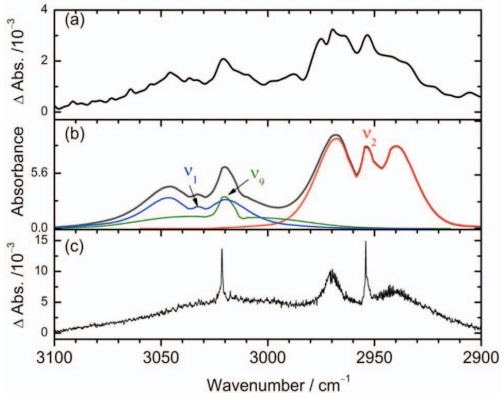

Fig. 10. Comparison of observed and simulated spectra of CH_3OO recorded under varied conditions. (a) Previously reported spectra recorded upon photolysis of a flowing mixture of CH_3I/O_2 (~1/100, 203 Torr, 281 K) at resolution 4 cm^{-1}.[41] (b) Spectra simulated at resolution 4 cm^{-1} (thick black line); individual bands of three vibrational modes are shown in thin grey lines. (c) Spectra recorded upon photolysis of a flowing mixture of CH_3COCH_3/O_2 (~1.6/99, 101 Torr, 298 K) at resolution 0.17 cm^{-1} using the second-generation system.

direct IR identification of even the simplest gaseous intermediate CH_2OO (formaldehyde oxide) has been reported. We recorded the transient infrared absorption spectrum of CH_2OO, produced from $CH_2I + O_2$ in a flow reactor, with the ss-FTIR technique.[45] The five bands observed at 849, 908, 1240, 1286, and 1435 cm^{-1} provide a definitive identification of this intermediate. The observed wavenumbers of the O–O stretching mode of CH_2OO near 908 cm^{-1} is much smaller than the wavenumbers of the corresponding modes of CH_3OO at 1117 cm^{-1} (Ref. 41) and $CH_3C(O)OO$ at 1102 cm^{-1},[42] determined with a similar technique (Table 2). The observed wavenumber of the C–O stretching mode near 1286 cm^{-1} is much larger than the corresponding value of CH_3OO at 902 cm^{-1} observed in a matrix[62] and 911 cm^{-1} observed in our second-generation system, indicating some double bond character. These observed vibrational wavenumbers imply that a zwitterion with a strengthened CO bond and a weakened OO bond rather than a diradical describes this intermediate more appropriately. The direct IR detection of CH_2OO will be very useful for kinetic and mechanistic investigations involving the Criegee mechanism.

4. Reactions of benzyl radical

Benzyl radical (C_6H_5) is the simplest aromatic radical; it plays an important role in organic synthesis, atmospheric chemistry and combustion chemistry. The reactions of C_6H_5 with CO, O_2, and SO_2 have been investigated with the ss-FTIR technique.

C_6H_5CO was generated from photolysis at 248 nm of acetophenone, $C_6H_5C(O)CH_3$, or via the reaction of phenyl radical (C_6H_5) with CO upon photolysis of C_6H_5Br at 248 nm.[43] An intense band near 1838 cm^{-1} and a weak band near 1131 cm^{-1} are assigned to the C=O stretching (ν_6) and mixed modes of the C–C stretching and C–H deformation (ν_{15}) of C_6H_5CO, respectively. Several secondary products, such as BrCO, $C_6H_5C(O)Br$, and $C_6H_5C(O)C_6H_5$, were also observed in the $C_6H_5Br/CO/N_2$ experiments; a corresponding kinetic analysis was performed.

The reaction of C_6H_5CO with O_2 was investigated.[44] Two intense bands near 1830 and 1226 cm^{-1} are assigned to the C=O stretching (ν_6) and C–C stretching mixed with C–H deformation (ν_{13}) modes and two weak bands near 1187 and 1108 cm^{-1} are attributed to the C–H deformation (ν_{14}) and O–O stretching/CH deformation (ν_{16}) modes of *syn*-$C_6H_5C(O)OO$, the benzoylperoxy radical. The secondary self-reaction of $C_6H_5C(O)OO$ generates $C_6H_5C(O)OOC(O)C_6H_5$. Observed bands of the aforementioned OO- and CO-containing species are summarized in Table 2.

Table 2. Comparison of observed vibrational wavenumbers of OO-stretching and CO-stretching modes of various imtermediates

	OO-stretch	CO-stretch	Ref.
t-ClC(O)OH		1808	38
c-ClC(O)OH		1883	38
t-$CH_3C(O)OO$	1102/1169	1851	42
c-$CH_3C(O)OO$	1078/1142	1862	42
syn-$C_6H_5C(O)OO$	1108	1830	44
C_6H_5CO		1838	43
CH_3OO	1117/1183	911[a]	41
CH_2OO	908	1286/1435	45

[a] unpublished work; 902 cm^{-1} in an Ar matrix.[62]

The reaction of C_6H_5 with SO_2 was studied because of its importance in organic synthesis.[37] Upon the irradiation at 248 nm of three flowing mixtures, $C_6H_5SO_2Cl$ in N_2, C_6H_5Cl and SO_2 in CO_2, and C_6H_5Br and SO_2 in CO_2, two transient features with origins at 1087.7 and 1278.2 cm^{-1} were assigned to the symmetric and antisymmetric SO_2-stretching modes of $C_6H_5SO_2$, respectively. When the mixture containing $C_6H_5Br/SO_2/CO_2$ was used to produce $C_6H_5SO_2$, two transient bands observed near 1186 and 1396 cm^{-1} at a subsequent reaction period were ascribable to $C_6H_5SO_2Br$, due to secondary reaction of $C_6H_5SO_2$ with Br.

SUMMARY

A step-scan time-resolved Fourier-transform spectrometer coupled with a multipass White cell as a reactor has been applied to characterize many reaction intermediates that are important in atmospheric chemistry; these gaseous IR spectra were unreported previously. The wide spectral coverage and adequate temporal resolution provide information on chemical kinetics, which, coupled with vibrational wavenumbers and IR intensities predicted quantum-chemically, aid in the assignments of observed absorption bands. The rotational contours of observed bands provide critical information for the assignments to distinguish conformers or isomers. Although other techniques using IR lasers might have sensitivity superior to this technique, the multiplex advantage of the ss-FTIR technique provides a wide spectral coverage for simultaneous detection of several species in the reaction system and is an excellent tool for exploring unknown species. The

spectra in the fingerprint region thus obtained provide valuable information on molecular structures and can be employed for direct probe and further investigations on chemical kinetics and reaction mechanisms.

ACKNOWLEDGEMENTS

National Science Council of Taiwan (Grants No. NSC102-2745-M009-001-ASP) and Ministry of Education, Taiwan ("Aim for the Top University Plan" of National Chiao Tung University) supported this work. The National Center for High-Performance Computing provided computer time.

REFERENCES

1. Fellgett, P. B. *J. Phys. Radium* **1958**, *19*, 187.
2. Jacquinot, P. *J. Opt. Soc. Am*. **1954**, *44*, 761.
3. Connes, J. *J. Phys. Radium* **1958**, *19*, 197.
4. Braiman, M. S.; Ahl, P. L.; Rothschild, K. J. *Proc. Nat. Acad. Sci. U S A* **1987**, *84*, 5221.
5. *Time-Resolved Vibrational Spectroscopy*, Springer Proceedings In *Physics 4*. Laubereau, A.; Stockburger, M., Eds.; Springer-Vetlag: Berlin, Germany, 1985.
6. Heard, D. E.; Brownsword, R. A.; Weston, D. G.; Hancock, G. *Appl. Spectros*. **1993**, *47*, 1438.
7. Sakai, H.; Murphy, R. E. *Appl. Opt.* **1978**, *17*, 1342.
8. Barowy, W.; Sakai, H. *Infrared Phys.* **1984**, *24*, 251.
9. Green, B. D.; Caledonia, G. E.; Murphy, R. E.; Robert, F. X. *J. Chem. Phys.* **1982**, *76*, 2441.
10. Hancock, G.; Heard, D. E. *Chem. Phys. Lett.* **1989**, *158*, 167.
11. Hartland, G. V.; Xie, W.; Dai, H.-L.; Simon, A.; Anderson, M. J. *Rev. Sci. Instrum*. **1992**, *63*, 3261.
12. Lin, S.-R.; Lin, S.-C.; Lee, Y.-C.; Chou, Y.-C.; Chen, I-C.; Lee, Y.-P. *J. Chem. Phys.* **2001**, *114*, 160.
13. Lin, S.-R.; Lin, S.-C.; Lee, Y.-C.; Chou, Y.-C.; Chen, I-C.; Lee, Y.-P. *J. Chem. Phys.* **2001**, *114*, 7396.
14. Lin, S.-R.; Lee, Y.-P. *J. Chem. Phys.* **1999**, *111*, 9233.
15. Wu, C.-Y.; Chung, C.-Y.; Lee, Y.-C.; Lee, Y.-P. *J. Chem. Phys.* **2002**, *117*, 9785.
16. Cheng, S.-S.; Wu, Y.-J.; Lee, Y.-P. *J. Chem. Phys.* **2004**, *120*, 1792.
17. Chen, K.-S.; Cheng, S.-S.; Lee, Y.-P. *J. Chem. Phys.* **2003**, *119*, 4229.
18. Wu, C.-Y.; Lee, Y.-P.; Ogilvie, J. F.; Wang, N. S. *J. Phys. Chem. A* **2003**, *107*, 2389.
19. Wu, C.-Y.; Lee, Y.-P.; Wang, N. S. *J. Chem. Phys.* **2004**, *120*, 6957.
20. Chen, H.-F.; Lee, Y.-P. *J. Phys. Chem. A* **2006**, *110*, 12096.
21. Tseng, C.-M.; Lee, Y. T.; Lin, M.-F.; Ni, C.-K.; Liu, S.-Y.; Lee, Y.-P.; Xu, Z. F.; Lin, M. C. *J. Phys. Chem. A* **2007**, *111*, 9463.
22. Chen, H.-F.; Liang, C.-W.; Lin, J. J.; Lee, Y.-P.; Ogilvie, J. F.; Xu, Z. F.; Lin, M. C. *J. Chem. Phys.* **2008**, *129*, 174303.
23. Bagchi, A.; Huang, Y.-H.; Xu, Z. F.; Raghunath, P.; Lee, Y. T.; Ni, C.-K.; Lin, M. C.; Lee, Y.-P. *Chem. Asian J*. **2011**, *6*, 2961.
24. Chen, H.-F.; Tsuchiya, S.; Lee, Y.-P. *J. Phys. Chem. A* **2009**, *113*, 3431.
25. Chiang, H.-C.; Wang, N. S.; Tsuchiya, S.; Chen, H.-T.; Lee,Y.-P.; Lin, M. C. *J. Phys. Chem. A* **2009**, *113*, 13260.
26. Huang, C.-K.; Xu, Z.-F.; Nakajima, M.; Nguyen, Hue M. T.; Lin, M. C.; Tsuchiya, S.; Lee, Y.-P. *J. Chem. Phys.* **2012**, *137*, 164307.
27. Uhmann, W.; Becker, A.; Taran, C.; Siebert, F. *Appl. Spectros.* **1991**, *45*, 390.
28. Xiao, Y.; Partha, R.; Krebs, R.; Braiman, M. *J. Phys. Chem. B* **2005**, *109*, 634.
29. Chen, P. Y.; Palmer, R. A.; Meyer, T. J. *J. Phys. Chem. A* **1998**, *102*, 3042.
30. Cowan, A. J.; Portius, P.; Kawanami, H.; Jina, O. S.; Grills, D. C.; Sun, X.-Z.; McMaster, J.; George, M. W. *Proc. Nat. Acad. Sci. U. S. A.* **2007**, *104*, 6933.
31. Vasenkov, S.; Frei, H. *J. Phys. Chem. A* **2000**, *104*, 4327.
32. Garczarek, F.; Gerwert, K. *Nature* **2006**, *439*, 109.
33. Chen, S.-H.; Chu, L.-K.; Chen, Y.-J.; Chen, I-C.; Lee, Y.-P. *Chem. Phys. Lett*. **2001**, *333*, 365.
34. Chu, L.-K.; Lee, Y.-P.; Jiang, E. Y. *J. Chem. Phys*. **2004**, *120*, 3179.
35. Chu, L.-K.; Han, H.-L.; Lee, Y.-P. *J. Chem. Phys*. **2007**, *126*, 174310.
36. Chu, L.-K.; Lee, Y.-P. *J. Chem. Phys*. **2006**, *124*, 244301.
37. Chu, L.-K.; Lee, Y.-P. *J. Chem. Phys*. **2007**, *126*, 134311.
38. Chu, L.-K.; Lee, Y.-P. *J. Chem. Phys*. **2009**, *130*, 174304.
39. Chu, L.-K.; Lee, Y.-P. *J. Chem. Phys*. **2010**, *133*, 184303.
40. Chen, J.-D.; Lee, Y.-P. *J. Chem. Phys.* **2011**, *134*, 094304.
41. Huang, D.-R.; Chu, L.-K.; Lee, Y.-P. *J. Chem. Phys*. **2007**, *127*, 234318.
42. Chen, S.-Y.; Lee, Y.-P. *J. Chem. Phys*. **2010**, *132*, 114303.
43. Lin, S.-Y.; Lee, Y.-P. *J. Phys. Chem. A* **2012**, *116*, 6366.
44. Golec, B.; Chen, J.-D.; Lee, Y.-P. *J. Chem. Phys*. **2011**, *135*, 224302.
45. Su, Y.-T.; Huang, Y.-H.; Witek, H. A.; Lee, Y.-P. *Science* **2013**, *340*, 174.
46. Eberhard, J.; Yeh, P.-S.; Lee, Y.-P. *J. Chem. Phys.* **1997**, *107*, 6499.
47. Uhmann, W.; Becker, A.; Taran, C.; Siebert, F. *Appl. Spectrosc.* **1991**, *45*, 390.
48. Nyquist, H. *AIEE Trans.* **1928**, *617*, 644.
49. White, J. U. *J. Opt. Soc. Am.* **1942**, *32*, 285.
50. Herres, W.; Gronholz, J. *Comp. Appl. Lab.* **1984**, *2*, 216.
51. Gaussian 09, Revision 7.0, Frisch, M. J.; Trucks, G. W.; Schlegel, H. B.; Scuseria, G. E.; Robb, M. A.; Cheeseman, J. R.; Scalmani, G.; Barone, V.; Mennucci, B.; Petersson, G. A.; Nakatsuji, H.; Caricato, M.; Li, X.; Hratchian, H. P.; Izmaylov, A. F.; Bloino, J.; Zheng, G.; Sonnenberg, J. L.; Hada, M.; Ehara, M.; Toyota, K.; Fukuda, R.; Hasegawa, J.;

Ishida, M.; Nakajima, T.; Honda, Y.; Kitao, O.; Nakai, H.; Vreven, T.; Montgomery, Jr., J. A.; Peralta, J. E.; Ogliaro, F.; Bearpark, M.; Heyd, J. J.; Brothers, E.; Kudin, K. N.; Staroverov, V. N.; Kobayashi, R.; Normand, J.; Raghavachari, K.; Rendell, A.; Burant, J. C.; Iyengar, S. S.; Tomasi, J.; Cossi, M.; Rega, N.; Millam, J. M.; Klene, M.; Knox, J. E.; Cross, J. B.; Bakken, V.; Adamo, C.; Jaramillo, J.; Gomperts, R.; Stratmann, R. E.; Yazyev, O.; Austin, A. J.; Cammi, R.; Pomelli, C.; Ochterski, J. W.; Martin, R. L.; Morokuma, K.; Zakrzewski, V. G.; Voth, G. A.; Salvador, P.; Dannenberg, J. J.; Dapprich, S.; Daniels, A. D.; Farkas, Ö.; Foresman, J. B.; Ortiz, J. V.; Cioslowski, J.; Fox, D. J. Gaussian, Inc., Wallingford CT USA, 2009.

52. PGOPHER. *A Program for simulating Rotational Structure*; Western, C. M., Univeristy of Bristol, UK, http://pgopher.chm.bris.ac.uk (version 7.1.108, released 13 Sept. 2010).
53. Stakhursky, V.; Miller, T. A. SpecView: Simulation and Fitting of Rotational Structure of Electronic and Vibronic Bands, In Proceedings of the 56th OSU International Symposium on Molecular Spectroscopy; Columbus, Ohio, USA, 2001.
54. Lee, Y.-P. *J. Chin. Chem. Soc.* **2005**, *52*, 641.
55. Bahou, M.; Huang, C.-W.; Huang, Y.-L.; Glatthaar, J.; Lee, Y.-P. *J. Chin. Chem. Soc.* **2010**, *57*, 771.
56. Tyndall, G. S.; Ravishankara, A. R. *Int. J. Chem. Kinet.* **1991**, *23*, 483.
57. Yin, F.; Grosjean, D.; Seinfeld, J. H. *J. Atmos. Chem.* **1990**, *11*, 309.
58. Zhu, L.; Bozzelli, J. W. *J. Phys. Chem. A* **2006**, *110*, 6923.
59. Frank, A. J.; Turecek, F. *J. Phys. Chem. A* **1999**, *103*, 5348.
60. Davis, S. R. *J. Phys. Chem.* **1993**, *97*, 7535.
61. James, F. C.; Kerr, J. A.; Simons, J. P. *J. Chem. Soc., Faraday Trans. 1* **1973**, *69*, 2124.
62. Nandi, S.; Blanksby, S. J.; Zhang, X.; Nimlos, M. R.; Dayton, D. C.; Ellison, G. B. *J. Phys. Chem. A,* **2002**, *106*, 7547.
63. Atkinson, R.; Baulch, D. L.; Cox, R. A.; Hampson, Jr., R. F.; Kerr, J. A.; Rossi, M. J.; Troe, J. *J. Phys. Chem. Ref. Data* **2000**, *29*, 167.
64. Jacox, M. E. *Chem. Phys.* **1982**, *69*, 407.

